



Universiteit
Leiden
The Netherlands

Electrolyte buffering species as oxygen donor shuttles in CO electrooxidation

Marcandalli, G.; Cecilio de Oliveira Monteiro, M.; Koper, M.T.M.

Citation

Marcandalli, G., Cecilio de Oliveira Monteiro, M., & Koper, M. T. M. (2021). Electrolyte buffering species as oxygen donor shuttles in CO electrooxidation. *Physical Chemistry Chemical Physics*. doi:10.1039/D1CP05030C

Version: Publisher's Version

License: [Licensed under Article 25fa Copyright Act/Law \(Amendment Taverne\)](#)

Downloaded from: <https://hdl.handle.net/1887/3248604>

Note: To cite this publication please use the final published version (if applicable).



Cite this: DOI: 10.1039/d1cp05030c

Electrolyte buffering species as oxygen donor shuttles in CO electrooxidation†

 Giulia Marcandalli, Mariana C. O. Monteiro and Marc T. M. Koper *

Electrolyte buffering species have been shown to act as proton donors in the hydrogen evolution reaction (HER). Analogously, we study here whether these electrolyte species may participate in other reactions by investigating CO electrooxidation (COOR) on a gold rotating disk electrode. This model system, characterized by fast kinetics, exhibits a diffusion-limited regime, which helps in the identification of the species dictating the diffusion-limited current. Through a systematic concentration dependence study in a variety of buffers, we show that electrolyte buffering species act as oxygen donor shuttles in COOR, lowering the reaction overpotential. A similar correlation between electrolyte and electrocatalytic activity was observed for COOR on a different electrode material (Pt). Probing the electrode–electrolyte interface by attenuated total reflection infrared spectroscopy (ATR-FTIR) and modelling the surface speciation to include the effect of the solution reactions, we propose that the buffer conjugated base generates the oxygen donor (*i.e.* OH[−]) through its acid–base reaction with water.

 Received 3rd November 2021,
 Accepted 7th December 2021

DOI: 10.1039/d1cp05030c

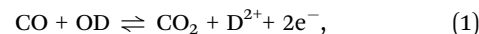
rsc.li/pccp

Introduction

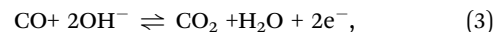
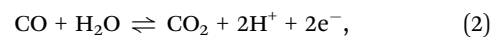
The electrochemical oxidation of CO (COOR) is of key importance, not only to deepen the fundamental understanding of electrochemical processes, but also for the implementation of electrocatalysis in energy-producing technology. In most of the relevant electrooxidation reactions exploited in fuel-cells, (adsorbed) CO acts as a reaction intermediate and/or as a poisoning species.¹ Furthermore, COOR is widely employed to probe the electrode/solution interface in terms of surface charge,^{2,3} electrochemical active surface area,⁴ surface pH⁵ and activity of the electrode surface.⁶

Depending on the CO adsorption energy,⁷ the electrode material may be poisoned by CO^{8–10} (*e.g.* Pt and Pd) or, in case of a weaker CO adsorption energy, exhibit high catalytic activity for COOR (*e.g.* Au).^{11,12} Typical COOR voltammograms on Au electrode display a kinetic-limited regime followed by a diffusion-limited regime for increasingly positive potential.¹¹ A strong pH dependence for COOR on Au has been observed,¹³ whose effects are not simply corrected by plotting the data on a pH-dependent potential scale. The low onset potential (*ca.* 0.2 V) in alkaline conditions (pH > 11) has been attributed to a self-promoting COOR mechanism, in which CO adsorption promotes the adsorption of its own oxidant (OH[−]/OH_{ad}).¹²

Considering a general oxygen donor (OD) for COOR, we may write:



expecting that the OD changes as a function of the pH (*i.e.* concentration of OH[−]). Specifically, we may consider that the OD switches from H₂O at acidic-neutral pH (eqn (2)) to OH[−] at more alkaline pH (eqn (3)).



In general, as the nature of the OD changes with pH, the mechanism of COOR may vary as well. Additionally, strongly adsorbing electrolyte anions have been proven to hinder COOR activity.¹⁴ Besides the marked pH and electrolyte dependence of COOR, most of the studies of COOR have been conducted either in strongly acidic or alkaline conditions without specific investigation of the role of the electrolyte anion. Recent works from our group highlighted the strong pH and electrolyte dependence of COOR both on Au¹⁵ and on Pt electrode.¹⁶ Interestingly, we detected the presence of two different peaks for COOR due to different diffusing species. These findings open the discussion on the nature of the oxygen donor for COOR, raising the questions: are H₂O and OH[−] the exclusive candidates for the role of oxygen donor in COOR? Or should other electrolytes species be considered as possible oxygen donors?

Leiden Institute of Chemistry, Leiden University, PO Box 9502, 2300 RA Leiden, The Netherlands. E-mail: m.koper@chem.leidenuniv.nl

† Electronic supplementary information (ESI) available. See DOI: 10.1039/d1cp05030c

In this paper, we probe the influence of the electrolyte composition, more specifically the anion, on COOR. To this end, we explored COOR on a Au rotating electrode in a variety of electrolytes and pH. Thus, we tested whether the insights gained for the trend between catalytic activity and electrolyte composition apply also for COOR on another metallic electrode (Pt). Subsequently, we investigated the surface population under COOR by attenuated total reflection infrared spectroscopy (ATR-FTIR). Finally, we built a model to elucidate how the presence of the buffer affects the concentration of species in the diffusion layer under COOR conditions. Altogether, we propose a mechanism for COOR in near-alkaline pH involving a solution reaction between the buffer conjugated base and water to form OH^- .

Experimental

Chemicals and materials

Electrolytes were prepared from H_2SO_4 (98%, Emsure, Merck), KClO_4 (99.995%, Aldrich Ultrapure), KHCO_3 (Emsure ACS, Merck), K_2CO_3 (99.995% trace metal basis, Sigma-Aldrich), KOH (99.99%, Sigma-Aldrich), H_3PO_4 (85%, Merck Suprapure), KH_2PO_4 (99.99%, Sigma-Aldrich), K_2HPO_4 ($\geq 99.999\%$, Honeywell Fluka), $\text{B}(\text{OH})_3$ (99.999% trace metal basis, Sigma-Aldrich), $\text{C}_6\text{H}_8\text{O}_7 \cdot \text{H}_2\text{O}$ ($\geq 99.998\%$ Traceselect, Honeywell Fluka), NH_3 (25%, Suprapure, Merck), using ultrapure water (MilliQ water, resistivity $\geq 18.2 \text{ M}\Omega \text{ cm}$). Prior to experiments, the electrolytes were purged for 20 minutes with Ar (6.0 purity, Linde) or CO (4.7 purity, Linde).

Experimental procedure

The glassware was cleaned in $1 \text{ g L}^{-1} \text{ KMnO}_4$ solution, rinsed with a dilute piranha solution and boiled in ultrapure water for five times. The electrochemical and spectroscopic measurements were carried out in a three-electrode configuration cell with a gold counter electrode (99.99% purity) and a reversible hydrogen electrode (RHE) or a Ag/AgCl electrode (KCl-saturated, Pine Research Instrumentation) as reference electrode. All the potentials are reported on the RHE scale, according to $E_{\text{RHE}} = E_{\text{Ag/AgCl}} + 0.199 \text{ V} + (0.059 \times \text{pH})$. A gold or platinum rotating disk electrode (RDE) was used as the working electrode ($\varnothing = 5.0 \text{ mm}$, Pine Research Instrumentation). The disk was inserted in the PEEK shroud and the assembled tip was polished with diamond suspensions of decreasing particle size (3, 1, 0.25 and $0.05 \mu\text{m}$) and sonicated in a solution of ultrapure water and ethanol. First, the gold (or platinum) working electrode was electrochemically characterized by cyclic voltammetry between 0.08 and 1.75 (1.6) V vs. RHE at 50 mV s^{-1} in $0.1 \text{ M H}_2\text{SO}_4$ (see Fig. S1 in the ESI†). The electrochemically active surface area (ECSA) was determined for gold by dividing the charge corresponding to the gold oxide reduction by $390 \mu\text{C cm}^{-2}$,¹⁷ and for platinum by dividing the charge corresponding to the hydrogen desorption region by $230 \mu\text{C cm}^{-2}$.¹⁸ Next, the gold (or platinum) catalytic activity for COOR in a given electrolyte was assessed by voltammetry

between 0.0 and the onset of oxygen evolution reaction (*ca.* 1.6 V vs. RHE) under forced convection. The electrolytes were prepared by adding different amounts of KOH or of an equimolar solution of the acid (AH) and conjugated base (A^-) of a given buffered electrolyte to a background of 0.1 M KClO_4 . The pH of the given electrolyte after 20 minutes CO purging was determined with a pH meter (SI Analytics Lab 855 Benchtop Meter). The voltammograms were compensated for 85% of the Ohmic drop. The Ohmic resistance was previously measured by electrochemical impedance spectroscopy (EIS) at 0.0 V vs. RHE. The measurements were performed using a IviumStat potentiostat (Ivium Technologies) and a Modulated Speed Rotator (Pine Research Instrumentation).

The FTIR measurements in the attenuated total reflectance configuration (ATR) were carried out using a Bruker Vertex 80v IR spectrophotometer with an incident angle of 60° and *p*-polarized infrared radiation. A gold thin film (*ca.* 60 nm thickness) was deposited by sputtering into a hemispherical ZnSe prism (MaTeck), which was previously mechanically polished ($0.05 \mu\text{m}$ diamond suspension). Cyclic voltammetry (CV) of the as-deposited film was performed between 0.0 and 1.5 V vs. RHE in the given electrolyte to assess the cleanliness of the setup and to enhance the roughness of the surface. Secondly, the solution was saturated with CO and a CV between 0.0 and 1.1 V vs. RHE was measured (see Fig. S7 in the ESI†). The reference spectrum was recorded at $E_{\text{ref}} = 0.0 \text{ V vs. RHE}$, after which the potential was increased in steps up to 1.1 V vs. RHE. Between each increment, the potential was biased back to E_{ref} and the reference spectrum was measured. In this way, we minimized the interference of spectral features due to changes in the prism and in the metallic film. The spectra are measured with a resolution of 4 cm^{-1} and are the average of 150 interferograms.

Results

Electrochemical measurements

We investigated the presence of different oxygen donors for bulk COOR by tuning the electrolyte composition using a Au rotating disk electrode. First, we studied the effect of increasing the concentration of OH^- on COOR activity. Starting from 0.1 M KClO_4 , as background electrolyte, we added increasing amounts of KOH. Fig. 1A shows the voltammetry of the gold disk at 50 mV s^{-1} and 1600 rpm for increasing OH^- concentration. We observe the presence of two separate diffusion-limited current regions. Throughout the paper, we will call the diffusion limiting current at lower potential (*ca.* 0.25–0.6 V_{RHE}) the 1st plateau, and the plateau current at more positive potential (*ca.* 0.6–1.3 V_{RHE}) the 2nd plateau. The 1st and 2nd current plateaus exhibit a different dependence on the electrolyte composition. Specifically, the 1st plateau current increases with the increase in OH^- concentration, while the current of the 2nd plateau remains constant. The 1st plateau current is zero in electrolyte not containing OH^- , is proportional to the concentration of OH^- for 0.1, 0.5 and 1.0 mM OH^- , and merges

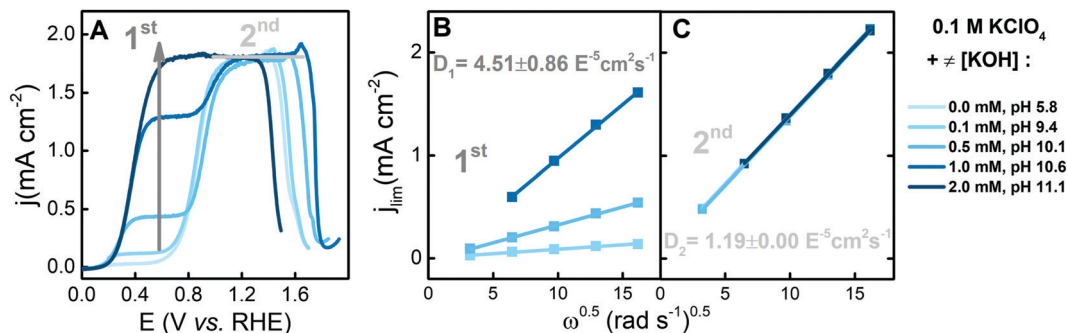


Fig. 1 (A) Voltammetry of the Au RDE electrode in CO-saturated 0.1 M KClO₄ of increasing concentration of KOH (0.0, 0.1, 0.5, 1.0 and 2.0 mM) at 50 mV s⁻¹ and 1600 rpm. Levich plot and the derived diffusion coefficient value for the 1st plateau (B) and for the 2nd plateau (C).

with the 2nd plateau current in 2.0 mM OH⁻. To understand the nature of the species leading to the diffusion limiting currents of the 1st and 2nd plateau, we performed a Levich analysis. According to the Levich equation,¹⁹ the diffusion limiting current (j_{lim}) is:

$$j_{lim} = 0.62nF\nu^{-1/6}D^{2/3}\omega^{1/2}c, \quad (4)$$

where n is the number of electrons transferred, F is the Faraday constant, ν is the kinematic viscosity of water, D is the diffusion coefficient, ω is the rotation rate and c is the bulk concentration. Fig. 1B and C show the Levich plots for the 1st and 2nd current plateaus, respectively, as extracted from the voltammetry at different rotation rates (see Fig. S2 in the ESI†). Knowing the bulk concentration, it is possible to derive the diffusion coefficient by the slope of the linear fit of j_{lim} vs. the square root of the rotation rate ($\omega^{0.5}$). The average derived diffusion coefficients are $4.51 (\pm 0.86) \times 10^{-5}$ and $1.19 (\pm 0.00) \times 10^{-5}$ cm² s⁻¹ for the 1st and 2nd limiting current, taking for the parameter c in eqn (4) the concentration of OH⁻ and CO, respectively. The comparison of the experimentally obtained and tabulated diffusion coefficients indeed indicates that the 1st plateau current is limited by the diffusion of OH⁻, while the 2nd is limited by the diffusion of CO (see Table S1 in the ESI†). This interpretation agrees with the pH dependence of the 1st plateau. We attribute the different plateaus to the different nature of the oxygen donor for COOR: in the 1st plateau the OD is OH⁻, while in the 2nd plateau it is H₂O. Considering that the bulk concentration of CO is 1 mM, the diffusion limiting species for COOR is the OD, only when [OD] < 1 mM. In aqueous electrolytes, the concentration of H₂O is large enough (55.5 M), that the diffusion limiting species for the 2nd plateau (with H₂O as the OD) is always CO. These results are in agreement with our findings for CO electrooxidation on platinum microelectrode.¹⁶

For potentials corresponding to the formation of 3D gold oxide (1.3–1.5 V) and subsequent onset of oxygen evolution reaction (OER), the COOR activity vanishes. As illustrated in Fig. 1A, this potential shifts to larger values for increasing [OH⁻], but at 2.0 mM OH⁻ it is shifted to markedly lower value. This pH dependence is consistent with the one reported for OER on gold polycrystalline by Yang *et al.*²⁰ The onset potential for OER at intermediate pH (4–10) increases with pH, while in alkaline conditions it decreases with pH, which

was ascribed to the presence of different gold oxide structures (α and β).

We continued the investigation of COOR in buffering electrolytes containing a variety of anions, spanning from mildly acidic to alkaline pH. Fig. 2 shows the voltammetry for bulk COOR on a gold RDE electrode in 0.1 M KClO₄ with the addition of an equimolar (AH/A⁻) concentration of given buffer species: (A) phosphate (pK_a 2.1), (B) citrate (pK_a 3.1), (C) phosphate (pK_a 7.1), (D) borate (pK_a 9.1), (F) bicarbonate

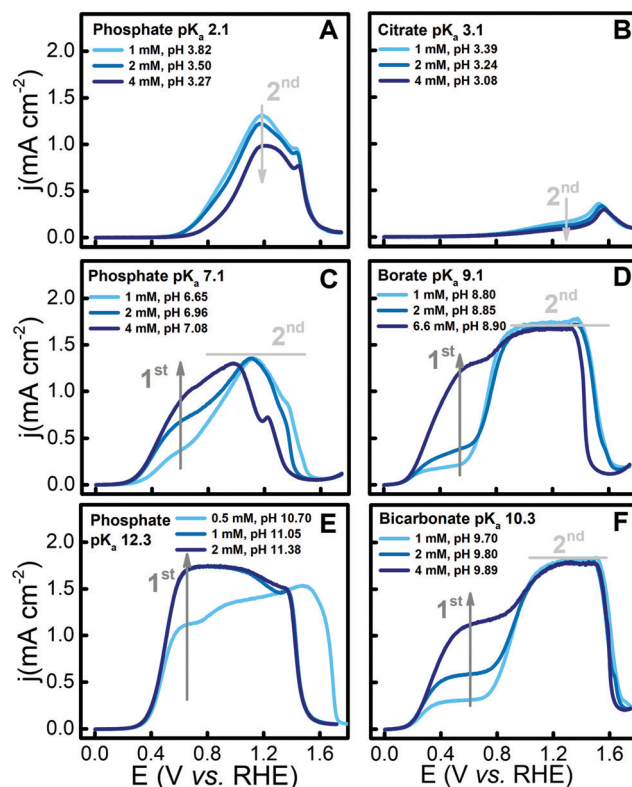


Fig. 2 Voltammetry of the Au RDE electrode in CO-saturated 0.1 M KClO₄ with the addition of equimolar solutions of (A) phosphate buffer H₃PO₄/KH₂PO₄, (B) citrate buffer C₆H₈O₇/KC₆H₇O₇, (C) phosphate buffer KH₂PO₄/K₂HPO₄, (D) borate buffer B(OH)₃/KB(OH)₄, (E) phosphate buffer K₂HPO₄/K₃PO₄ and (F) bicarbonate buffer KHCO₃/K₂CO₃ at 50 mV s⁻¹ and 1600 rpm.

(pK_a 10.3) and (E) phosphate (pK_a 12.3). For some electrolytes, we can still distinguish the presence of two current plateaus, while for others only a COOR current in the potential window of the 2nd feature is present. In borate and bicarbonate containing solutions, the 2nd plateau is independent of the concentration of the buffering electrolytes and comparable to the one measured in pure perchlorate (see Fig. 1A). By contrast, in phosphate and citrate electrolytes, the current of the 2nd plateau is lower. Presumably, there is a competition between the adsorption of electrolyte anions and COOR, which leads to a suppression of COOR current in electrolytes with strongly adsorbing anions,¹⁴ *i.e.* phosphate and citrate.

Importantly, the 1st COOR plateau emerges only in near neutral or alkaline solutions (phosphate pK_a 7.1 and 12.3, borate pK_a 9.1 and bicarbonate pK_a 10.3) and its current scales linearly with the concentration of the buffering electrolytes (Fig. 3B). Even if the 1st plateau was previously ascribed to COOR by OH^- , in this case the increase in pH is not sufficient to explain the increase in current. Yet, as illustrated in Fig. 3A the 1st plateau current follows Levich and is still a diffusion-limited process. From the rotation rate and concentration dependence study (see Fig. 3A and B, respectively), we derived the diffusion coefficient for the species leading to the limiting COOR of the 1st plateau in phosphate (pK_a 7.1), borate and bicarbonate electrolyte (taking for the parameter c in eqn (4) the concentration of A^- , see ESI† for more details). We excluded the analysis of the diffusion coefficient in the phosphate buffer with a pK_a of 12.3, as for this pH (11) there is already a large concentration of OH^- in solution. As shown in Fig. 3C, the obtained diffusion coefficients are one order of magnitude lower than the one previously calculated for COOR limited by the diffusion of OH^- , but also lower compared to the tabulated values for the different electrolyte species (see Table S1 in the ESI†). Online electrochemical mass spectrometry (OLEMS) measurement confirms that the product of COOR is still CO_2 under these experimental conditions (see Fig. S6 in the ESI†). In fact, the value of the ratio of the peaks current (1st/2nd) from voltammetry corresponds to the one obtained from the CO_2 signal [m/z 44] at potential coinciding with 1st and 2nd peaks.

Hence, the 1st current plateau relates to COOR to CO_2 and it involves the participation of the buffering electrolyte, as the 1st plateau current scales linearly with the concentration of the buffer (*e.g.* A^-). The near one order of magnitude difference between the derived diffusion coefficient and the tabulated one may be the result of a process involving first a chemical equilibrium followed by electron transfer.^{21, 22} A more detailed discussion about the origin of the discrepancy in the value of the diffusion coefficient will be given in the section about the “Microkinetic modelling”.

Up to now the measurements were performed in electrolytes containing equimolar solutions of AH and A^- to minimize pH changes, however we expect that the A^- is the buffering species directly involved in the rise of the 1st plateau. To test our hypothesis we performed the COOR in electrolytes selectively containing only AH or only A^- . Fig. 4 A displays the limiting current as a function of rotation rate for the 1st COOR plateau in electrolytes containing 1 mM of equimolar $\text{KHCO}_3/\text{K}_2\text{CO}_3$, 0.5 mM KHCO_3 and 0.5 mM K_2CO_3 . Corroborating our hypothesis, the limiting current in electrolytes containing A^- is comparable to the one containing both AH and A^- , while in purely AH-containing solution the current is almost zero. The small difference between the limiting current in 1 mM $\text{KHCO}_3/\text{K}_2\text{CO}_3$ and 0.5 mM K_2CO_3 originates mainly from the difference in the bulk pH. Adding just A^- (compared to equimolar AH/ A^-) results in a larger bulk pH, hence in higher COOR currents. Now that we established that the OD is directly correlated to the concentration of A^- , we investigate whether A^- is the direct OD or rather the OD is provided by A^- through its acid-base reaction with water. Therefore, we performed COOR in an ammonium buffer ($\text{NH}_4\text{ClO}_4/\text{NH}_3$, pK_a 9.2), which does not contain any oxygen atom (see Fig. S11, ESI†). As illustrated in Fig. 4B, the limiting current of the 1st COOR plateau still increases linearly with the concentration of the ammonium buffer. This observation leads us to exclude that the A^- is the direct OD in COOR.

We probed whether the role of A^- to supply the OD for COOR also applies to other metal electrodes. Recently, we reported that COOR on Pt electrode also presents the two

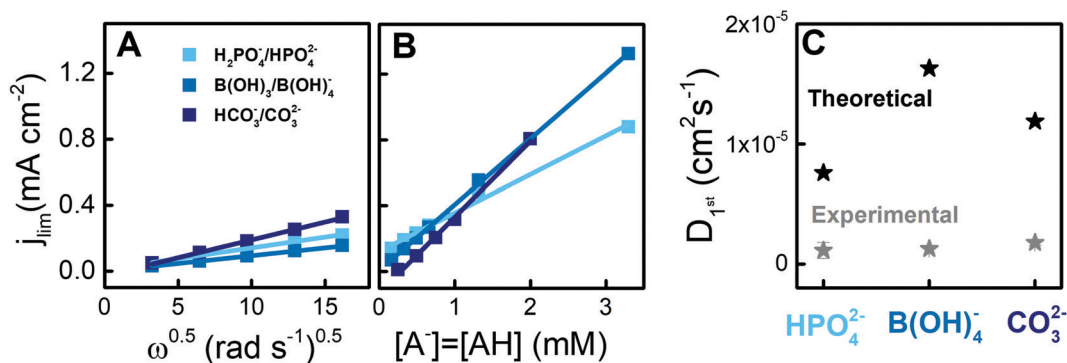


Fig. 3 (A) Levich plot for the 1st COOR plateau in 0.1 M KClO_4 + 0.66 mM $\text{KH}_2\text{PO}_4/\text{K}_2\text{HPO}_4$, 0.66 mM $\text{B(OH)}_3/\text{KB(OH)}_4$ and 1 mM $\text{KHCO}_3/\text{K}_2\text{CO}_3$ as measured in Fig. S3 (ESI†). (B) The limiting current of the 1st COOR plateau as a function of the concentration of the conjugated base (A^-) of the buffer (and the corresponding equimolar concentration of AH) as measured in Fig. 2. (C) The average diffusion coefficient values as derived from the linear fitting of (A) and (B) compared to the theoretical values.

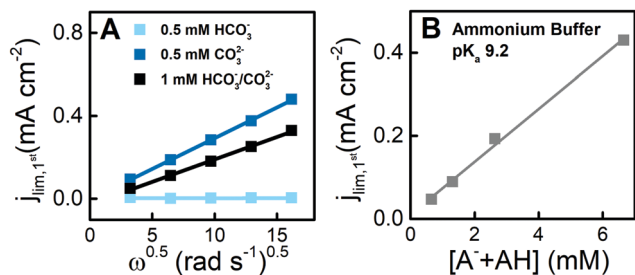


Fig. 4 (A) Levich plot for the 1st COOR plateau in 0.1 M KClO_4 with the addition of 0.5 mM KHCO_3 , 0.5 mM K_2CO_3 and 1 mM $\text{KHCO}_3/\text{K}_2\text{CO}_3$ (equimolar) as measured in Fig. S4 and in Fig. S3 (ESI †). (B) The limiting current of the 1st COOR plateau as a function of the concentration of the ammonium buffer ($\text{NH}_4\text{ClO}_4/\text{NH}_3$) in a 0.1 M KClO_4 supporting electrolyte as measured at 50 mV s^{-1} and 1600 rpm in Fig. S11 (ESI †).

distinct potential region oxidation waves for increasing concentration of OH^- , which were assigned to the change in the OD nature from H_2O to OH^- . Hence, we studied COOR in buffering electrolytes on Pt RDE electrode under the same experimental conditions used for Au. Fig. 5 displays the voltammograms for COOR on a Pt RDE in pure 0.1 M KClO_4 and with the addition of 2 mM of equimolar $\text{KH}_2\text{PO}_4/\text{K}_2\text{HPO}_4$, $\text{B}(\text{OH})_3/\text{KB}(\text{OH})_4$ and $\text{KHCO}_3/\text{K}_2\text{CO}_3$. In agreement with the behaviour observed for COOR on Au electrode, also on Pt we observe two separate COOR oxidation peaks. The same electrolyte dependence for the two separate COOR oxidation waves is also found. Namely, the 2nd peak is independent of the electrolyte composition, while the 1st peak is present only in electrolytes containing the buffering species and its current is proportional to the buffer concentration (see Fig. S12 in the ESI †). Hence, analogously to the Au surface, we attribute the difference in the two COOR peaks to the different nature of the OD. For the 1st peak the OD is provided from A^- through its acid–base reaction, while for the 2nd peak H_2O dissociative adsorption into the surface provides the OD. However, there are clear differences in the voltammograms of COOR on Au and Pt, which are primarily due to the distinctive character of the CO adsorption energy. On Pt, the CO adsorption energy is larger than on Au, and as a

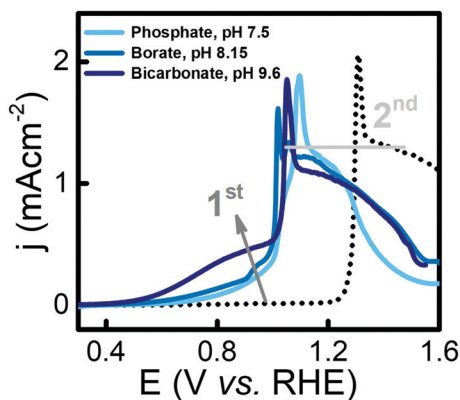


Fig. 5 Voltammetry of the Pt RDE electrode in CO-saturated 0.1 M KClO_4 (dotted line) with the addition of equimolar 2 mM $\text{KH}_2\text{PO}_4/\text{K}_2\text{HPO}_4$, $\text{B}(\text{OH})_3/\text{KB}(\text{OH})_4$, $\text{KHCO}_3/\text{K}_2\text{CO}_3$ at 50 mV s^{-1} and 1600 rpm.

consequence a CO adlayer is formed on the Pt surface at low positive potential. As the potential is increased, CO_{ad} is oxidatively removed, originating the characteristic sharp CO stripping peak. The potential of the CO stripping is less positive in buffering-containing electrolytes (1.05 V) compared to a pure KClO_4 solution (1.3 V), as the CO binding energy may change in different electrolytes. The difference in the CO binding energy also explains why for COOR on Au, in the absence of strongly adsorbing anions, we observe a purely diffusion-limited current plateau and, by contrast, on Pt the current is mostly limited by the rate of CO desorption.

Infrared spectroscopic measurements

We investigated by ATR-FTIR the origin of the 1st COOR on a gold thin film electrode in the buffering electrolytes, *i.e.* phosphate (pK_a 7.1) and bicarbonate buffer. For comparison, we also measured the infrared spectra in 0.1 M KClO_4 , in which the 1st plateau is absent, and in 0.1 M $\text{KClO}_4 + 2 \text{ mM OH}^-$, in which the 1st plateau is present and due to COOR by OH^- . Fig. 6 shows the infrared spectra in the various electrolytes during COOR at potential (A) 0.5 V corresponding to the 1st plateau and (B) 0.9 V corresponding to the 2nd plateau. The full series of infrared spectra for increasing positive potential (from 0.3 to 1.1 V) are shown in Fig. S10 in the ESI † . The spectra were measured in transmittance mode and the background spectrum recorded at 0.0 V (E_{ref}) was subtracted. Hence, a positive infrared band corresponds to the consumption, desorption, or change in the dipole moment orientation, of that species respect to E_{ref} .

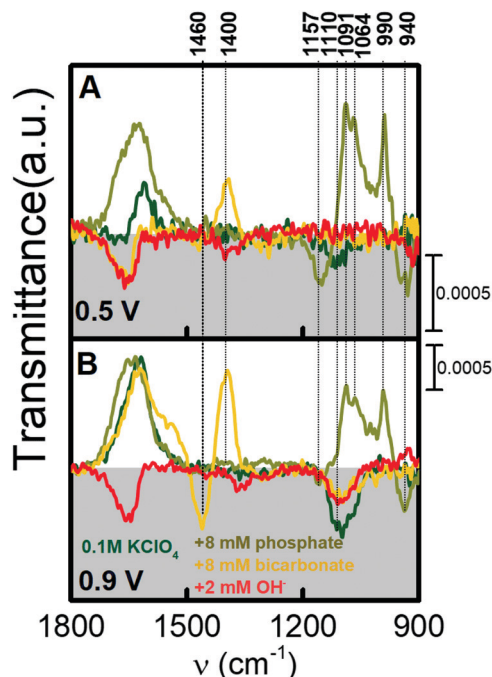


Fig. 6 ATR spectra of a Au thin film during COOR in CO-saturated 0.1 M KClO_4 , 0.1 M $\text{KClO}_4 + 8 \text{ mM KH}_2\text{PO}_4/\text{K}_2\text{HPO}_4$, 0.1 M $\text{KClO}_4 + 8 \text{ mM KHCO}_3/\text{K}_2\text{CO}_3$ and 0.1 M $\text{KClO}_4 + 2 \text{ mM KOH}$ biased at (A) 0.5 and (B) 0.9 V. The background spectra was measured at 0.0 V.

At 0.5 V (see Fig. 6A), we observe positive-going bands characteristic of buffer solution species, 1087 and 990 cm^{-1} in phosphate and 1400 cm^{-1} in bicarbonate-containing electrolytes. Indeed, these modes are comparable to the ones measured in the transmission spectra of HPO_4^{2-} (1078, 990 cm^{-1}) and CO_3^{2-} (1390 cm^{-1}) (see Fig. S8 in the ESI†). Correspondingly, we measured negative-going bands ascribable to solution H_2PO_4^- at 1157 and 940 cm^{-1} . The observed small differences in the wavenumber of the peaks measured during COOR compared to the ones measured in the transmission spectra is due to the overlapping of different modes with opposite sign and similar vibrational energy. Overall, in buffering-containing electrolytes at the potential corresponding to the 1st COOR plateau, we observe the consumption of solution A^- and the formation of solution AH. Concerning adsorbed CO, we observed the presence of CO_{top} at *ca.* 2010 cm^{-1} and $\text{CO}_{\text{bridge}}$ at *ca.* 1860 cm^{-1} as bipolar bands (see Fig. S9 in the ESI†), for potentials more positive than 0.4 and 0.5 V, respectively.

At 0.9 V (see Fig. 6B), we detected a positive increase in the water bending (δ_{HOH}) region at 1610–1620 cm^{-1} in all solutions, except in 2 mM KOH. The observed shift to lower wavenumber of δ_{HOH} at 1620 cm^{-1} compared to bulk water (1645 cm^{-1}) is characteristic of a decrease in the hydrogen-bonding network of interfacial water.^{23,24} This shift has been ascribed to the interaction between the oxygen lone-pair orbital of the water molecule and the electrode surface.²³ We argue that the consumption of weakly hydrogen-bonded water at 1620 cm^{-1} and in the water stretching region (3400–3500 cm^{-1} see Fig. S10A, C and D in the ESI†) confirms that H_2O is the OD at the potential corresponding to the 2nd plateau.

Moreover, at 0.9 V we also detect the presence of negative-going bands due to the specific adsorption of the electrolyte species. Specifically, the band at *ca.* 1110 cm^{-1} is ascribed to adsorbed perchlorate²³ and the band at *ca.* 1460 cm^{-1} to adsorbed carbonate.²⁵ In the Stern layer, the surface coverage for specific anion adsorption increases for increasing positive potential, especially around the potential of zero charge (E_{pzc}). Considering that $E_{\text{pzc}} = 0.412 + (0.059 \times \text{pH})$, it is reasonable to propose that specific anion adsorption is relevant at the potential corresponding to the 2nd COOR plateau. Importantly, the specific adsorption of buffering anion leads to a change in the pK_a of adsorbed species compared to the bulk, for both phosphate²⁶ and bicarbonate²⁷ electrolytes. The pK_a of AH/A^- shifts to lower value, as AH deprotonates upon adsorption leading to A_{ad} .²⁶ In our measurements, we could not clearly detect the specific adsorption of phosphate ions, which was reported to be at 1117 and 940 cm^{-1} for $\text{HPO}_{4,\text{ad}}$ and 1091 cm^{-1} for $\text{PO}_{4,\text{ad}}$. This may be due to the similar wavenumber of adsorbed and solution species, consumed during COOR, leading to a convolution of different modes in the region between 1120 and 1030 cm^{-1} . Nonetheless, we propose that the change in the surface acid–base equilibrium does not relate to the observed electrolyte dependence for COOR, as it takes place in the potential regime where H_2O is the OD. More relevant at this potential, it is instead the competition between specific anion

adsorption and H_2O adsorption leading to a decrease in the COOR activity (as described in the previous section).

Microkinetic modelling

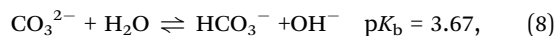
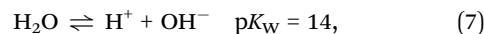
We built a model to capture the effect of the homogeneous buffer reactions on the concentration gradient developed in the diffusion layer in bicarbonate/carbonate solutions. For each species (i), the variation in the concentration over time (t) depends on the diffusion, the convection and the rate of the homogeneous reactions R_i according to:

$$\frac{\partial c_i}{\partial t} = D_i \frac{\partial^2 c_i}{\partial x^2} - v \frac{\partial c_i}{\partial x} + R_i, \quad (5)$$

where c_i (mol dm^{-3}) is the concentration, D_i ($\text{m}^2 \text{s}^{-1}$) is the diffusion coefficient and v (m s^{-1}) is the convective velocity. The diffusion term is expressed by the Fick's law.¹⁹ The convective velocity (v) is expressed as a function of the rotation speed across the distance (x) from the surface ($x = 0$) as:

$$v = -0.51\omega^{1/2}\nu^{-1/2}x^2 \quad (6)$$

where ω (rad s^{-1}) is the rotation speed frequency, ν ($\text{m}^2 \text{s}^{-1}$) is the kinematic viscosity of the solution and x (m) is the distance from the electrode surface. The homogeneous reactions included in the models are the self-ionization of water (eqn (7)) and the acid–base reactions of the buffer (eqn (8) and (9)).



Thus, we built a system of four partial differential equations (PDEs) expressing the variation in c_i for OH^- , H^+ , CO_3^{2-} and HCO_3^- . The system of PDEs was solved for given initial conditions (at $t = 0$, $c_i = c_{i,\text{bulk}}$) and boundary conditions. At the diffusion layer/bulk (right) boundary, we set that $c_{i,\text{right}} = c_{i,\text{bulk}}$. At the diffusion layer/electrode boundary (left boundary), at steady-state the flux of i is equal to the rate at which i is consumed/produced by the electrochemical reaction. In our model, we consider that the only OD for COOR is OH^- , according to eqn (3). Hence, we write that the rate at which OH^- is consumed is given by the rate of COOR (j_{COOR}) expressed in a Butler–Volmer form:

$$D_{\text{OH}^-} \frac{\partial c_{\text{OH}^-}}{\partial x} = -\frac{2j_{\text{COOR}}}{nF} = -2kc_{\text{OH}^-} \exp\left[\frac{\alpha_{\text{eff}}F(E - E_{\text{eq}}^0)}{RT}\right], \quad (10)$$

where n the number of electron transferred is 2, c_{OH^-} is the surface concentration of OH^- , k the reaction rate is $1.67 \times 10^{-7} \text{ m s}^{-1}$, $\alpha_{\text{eff}} (= \alpha n)$ the effective transfer coefficient is 1 and E_{eq}^0 the CO_2/CO standard equilibrium potential is -0.52 V vs. SHE. The reaction rate was determined by Koutecký–Levich analysis of COOR in 1 mM OH^- (see Fig. S14 in the ESI†), while a transfer coefficient (α) of 0.5 was assumed given an observed

Tafel Slope of *ca.* 120 mV dec⁻¹ (see Fig. S15 in the ESI†). On the other hand, as the proton and the buffering species are not directly consumed by the electrochemical reaction, it follows that at the left boundary:

$$D_{\text{H}^+} \frac{\partial c_{\text{H}^+}}{\partial x} = 0, \quad (11)$$

$$D_{\text{CO}_3^{2-}} \frac{\partial c_{\text{CO}_3^{2-}}}{\partial x} = 0, \quad (12)$$

$$D_{\text{HCO}_3^-} \frac{\partial c_{\text{HCO}_3^-}}{\partial x} = 0. \quad (13)$$

The system of PDEs was solved with MATLAB R2020 over a spacemesh x large enough to contain the diffusion layer ($x = 10^{-4.5}$ m at 1600 rpm). Details about the values of the parameters used in the model are given in the ESI†

Based on the electrochemical results obtained for the 1st COOR plateau on Au RDE in buffering electrolytes, we employed the model to consider the ability of the buffer to supply the OH⁻ at the electrode surface. Firstly, we limited the model to the case of bicarbonate/carbonate-containing electrolytes, considering the contribution of homogeneous reactions 7, 8 and 9 and reaction 3 as the only electrochemical reaction. For a given bulk pH of 10.33 (coinciding with the buffer p*K*_a), we investigated the effect of the buffer concentration (equimolar HCO₃⁻/CO₃²⁻) on the concentration of OH⁻ at the surface, and hence on the COOR current. Fig. 7 shows the simulated surface concentration of (A) OH⁻ and (B) HCO₃⁻ and CO₃²⁻ for different bicarbonate buffer concentration as a function of potential. At a given potential, the surface concentration of OH⁻ increases for increasing buffer concentration. Proportionately (as shown in Fig. 7B), CO₃²⁻ is converted into HCO₃⁻ for increasing potential. It follows that the j_{COOR} , calculated according to eqn (10), scales with the buffer concentration, as a consequence of the increasing availability of OH⁻ at the surface. For the mass transport limiting current, the surface concentrations of OH⁻ and the buffer conjugated base CO₃²⁻ are zero. Indeed, CO₃²⁻ has been completely converted into HCO₃⁻ according to reaction (8), whose reaction equilibrium is shifted to the right. Simultaneously, the consumption of OH⁻ by COOR triggers the homogeneous reaction of the buffer

conjugated base (A⁻) with water to produce more OH⁻ at the surface. As the electrochemical reaction rate increases exponentially with the potential, the homogeneous reaction is forced out of equilibrium (see Fig. S18A in the ESI†), and the mass transport limiting current is reached once all the A⁻ is converted into AH. At these potentials, the limiting current is dictated by the diffusion of CO₃²⁻ to the surface and by the rate at which OH⁻ is generated by reaction (8), as supported by modelling in the next paragraph.

Fig. 8A shows how the COOR diffusion limiting current $j_{\text{lim,A}^-}$ (with the contribution of OH⁻ itself subtracted) scales with the diffusion coefficient of A⁻, in this case CO₃²⁻. Reasonably, as described by Levich (eqn (4)), under diffusion limitation $j_{\text{lim,A}^-}$ scales linearly with $D^{2/3}$ and with the square root of the rotation rate (see Fig. S16A in the ESI†). Extrapolation of the diffusion coefficient from the simulated voltammograms, according to eqn S2 (ESI†) with c given by the bulk concentration of CO₃²⁻, results in a diffusion coefficient of 1.95×10^{-6} cm² s⁻¹. The latter value is comparable to the experimentally derived one (see Fig. 3) and almost one order of magnitude lower than the theoretical diffusion coefficient of CO₃²⁻ (see Table S1, ESI†).

To understand the effects of the thermodynamics and kinetics of acid–base reactions on $j_{\text{lim,A}^-}$, we extended our model to the full pH range by considering a general acid/base buffering couple (AH/A⁻):



with $K_a \times K_b = K_w$. To work at equimolar concentration of AH and A⁻, the pH should equal the p*K*_a; it follows that p*K*_b = 14 - pH. Hence, varying the pH we simulated the COOR diffusion limiting current with and without 2 mM AH/A⁻. We then obtained $j_{\text{lim,A}^-}$ subtracting the contribution of OH⁻ from the total diffusion limiting current in the presence of AH/A⁻ at the same pH. Fig. 8B illustrates how $j_{\text{lim,A}^-}$ varies with the p*K*_b (pH). We identified three different regimes describing the relation between $j_{\text{lim,A}^-}$ and the p*K*_b:

- I regime p*K*_b > 9 (pH < 5): $j_{\text{lim,A}^-}$ is zero independently of p*K*_b;

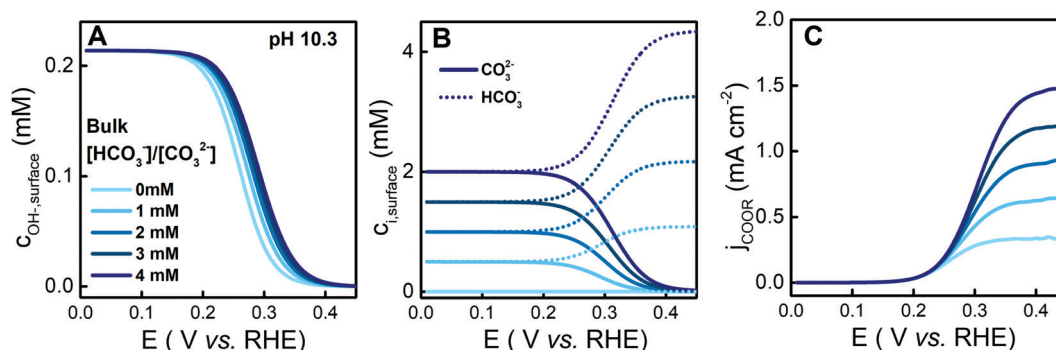


Fig. 7 Simulated surface concentration of (A) OH⁻ and (B) HCO₃⁻ and CO₃²⁻ at different concentration (0, 1, 2, 3 and 4 mM) of equimolar HCO₃⁻/CO₃²⁻ at pH 10.33 at 1600 rpm and 50 mV s⁻¹. (C) Corresponding simulated voltammograms for j_{COOR} according to eqn (10).

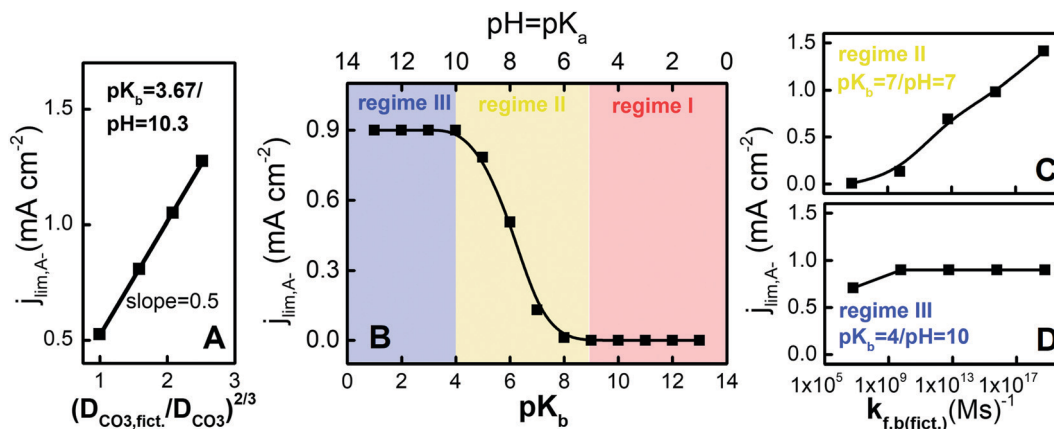


Fig. 8 Dependence of the COOR diffusion limiting current (A) on the diffusion coefficient of CO_3^{2-} , (B) on the equilibrium constant to generate OH^- (reaction (14)), and (C) and (D) on the forward rate constant of reaction 14. Values are obtained from simulations in equimolar 2 mM AH/A^- at 50 mV s^{-1} and 1600 rpm.

- II regime $4 < pK_b < 9$ ($6 < \text{pH} < 10$): $j_{\text{lim,A}^-}$ increases for decreasing pK_b ;
- III regime $pK_b < 4$ ($\text{pH} > 10$): $j_{\text{lim,A}^-}$ is constant and independent of pK_b .

Then, we evaluated how the kinetics of reaction (14) ($k_{f,b}$) affects $j_{\text{lim,A}^-}$ in regime II (Fig. 8C) and in regime III (Fig. 8D). For intermediate pH (regime II), the free concentration of OH^- is low and $j_{\text{lim,A}^-}$ highly depends on $k_{f,b}$, being reaction (14) out of equilibrium in the diffusion layer. For alkaline pH values (regime III), $j_{\text{lim,A}^-}$ exhibits no dependence on the kinetics of the acid–base reaction, except for $k_{f,b}$ values lower than $6 \times 10^9 \text{ (Ms)}^{-1}$. For increasing OH^- concentration, reaction 14 is mostly at equilibrium in the diffusion layer, explaining why $j_{\text{lim,A}^-}$ is independent of the pK_b in regime III.

Because of a mixed diffusion limitation in both OH^- and A^- , the “effective diffusion layer thickness” (δ_{eff}) is governed by the contribution of the diffusion velocity of each species weighted for their concentration profiles. In modelling the surface ion speciations for hydrogen evolution and oxidation reaction on platinum, Auinger *et al.* used a pH-dependent δ_{eff} , which was calculated given the average diffusion velocity of H^+ and OH^- ions weighted for their bulk concentrations.²⁸ Due to the high reversibility of the reactions studied, and fast kinetics of the homogeneous reactions involved, they assumed stationary conditions and they solved the mass transport equation analytically. Even if their model was able to catch local pH trends for such a well-defined system, it could not be extended to electrochemical processes with a more sluggish kinetics. By contrast, considering OH^- diffusion layer, in Fig. S16C (ESI[†]) we show how δ_{sim} changes with the $\text{HCO}_3^-/\text{CO}_3^{2-}$ buffer concentration for a given bulk pH, by solving the PDEs in a non-stationary system using Neumann boundary conditions. The buffering reaction (8) is slightly out of equilibrium close to the reaction plane (see Fig. S18C in the ESI[†]), and the equilibrium is then re-established at intermediate distances from the electrode surface. These complex ions concentration profiles, co-regulated by the rate of the electrochemical and chemical reactions weighted for the diffusion velocity of the different species

involved, may explain why extrapolation of the diffusion coefficients from simple Levich analysis leads to erroneous values. All together, COOR is limited by the diffusion of both OH^- and CO_3^{2-} , even if the reactant is OH^- . The higher flux of OH^- due to the contribution of CO_3^{2-} diffusion results in a higher diffusion limited current. The simulations highlight how the buffer species increase the effective flux of OH^- in the diffusion layer and depict a COOR mechanism involving a fast pre-equilibrium in solution to generate OH^- .

Discussion

The electrochemical and infrared results collected for COOR on a gold electrode in electrolytes containing buffering species with pK_a ranging between 7.1 and 10.3, together with the microkinetic modelling, indicate that for the 1st COOR plateau:

- The current is limited by the diffusion of the OD to the electrode surface, as it follows Levich equation (see Fig. 3A);
- The OD is a species, whose concentration relates to the concentration of the buffering electrolytes (see Fig. 3B). Still, the OD is not directly the buffering species as the derivation of the diffusion coefficient leads to a value that is one order of magnitude lower than the tabulated one (see Table S1 in the ESI[†]);
- The difference between the experimentally derived and the theoretical diffusion coefficient is due to a mechanism involving a solution reaction to form the OD preceding the electrochemical step (as corroborated by the simulations);
- A^- in solution is consumed and AH is formed (according to infrared data see Fig. 6).

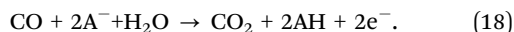
Based on these observations, we suggest that under the studied experimental conditions the OD for the 1st COOR plateau is delivered to the surface by diffusion of A^- , which through its acid–base reaction with H_2O releases an OH^- . The generated OH^- then adsorbs on the electrode surface (OH_{ad}). In such a way, A^- provides the OD leading to the low overpotential COOR plateau (1st) compared to the one observed at more

positive potential (2nd), requiring the activation of H₂O as the OD.

According to the widely reported Langmuir–Hinshelwood mechanism for COOR, we may write the following reactions pathway for the 1st COOR plateau in the presence of buffering species:



The complete COOR equation with A⁻ delivering the OD is then as follows:



Alternatively, we may write eqn (16) not as a solution reaction, but as an acid–base equilibrium involving adsorption of A⁻ according to:



Yet, the infrared spectroscopy data and the nature of the diffusion limiting current explained with the modelling suggest that the pathway going through eqn (16) is most likely. Consistently, the electrolyte-activity dependence for COOR is not surface-dependent and similar results were observed for both Au and Pt electrodes. Hence, the 1st COOR plateau current is limited by the rate at which A⁻ diffuses to the surface and by the rate at which OH⁻ is generated by the acid–base reaction of A⁻ with water.

Generalizing the role of A⁻ to supply the OD for other electrooxidation reaction, in the case of a negatively charged substrate (e.g. NO₂⁻) the competition between adsorption of the reactant molecules and the buffering anion should be considered. However, CO is a common intermediate of many electrooxidation pathways (e.g. methanol and ethanol electro-oxidation) and future investigations of the role of A⁻ in the electrooxidation of more complex molecules would be of interest.

Conclusions

By investigating COOR on different metallic surfaces (Au and Pt), we delineated the relationship between the electrolyte nature and the catalytic activity. We identified two COOR potential-regimes, characterized by the distinct nature of the OD. At less positive potential (1st regime), the OD is OH⁻, at higher potential (2nd regime), the OD is H₂O. The OH⁻ is either free OH⁻ in solution (for alkaline pH) or OH⁻ generated at the interface by the homogeneous reaction of A⁻ with water (for intermediate pH values). Reasonably, COOR by OH⁻ requires a lower overpotential compared to the pathway involving H₂O dissociation. From a fundamental perspective, these findings show in detail how the buffer species, through their ability to increase the effective diffusive flux of reactant (e.g., OH⁻), are decisive actors in determining electrocatalytic currents in near-neutral pH.

The role of the electrolyte buffer conjugated base to promote the electrooxidation process could be compared to the increase in activity achieved through electrode optimization by alloying noble metals with more oxophilic materials (e.g. Ni, Sn, Ru and Rh).^{29–31} This analogy provides an outlook on how not only electrode engineering, but also electrolyte engineering helps to steer the electrocatalytic activity in the desired way. Besides, understanding of electrochemistry in buffering-containing electrolytes with an intermediate pH is critical to the further development for cheaper and non-noble metal electrocatalysts, which are not stable at more extreme pH values.

Conflicts of interest

There are no conflicts to declare.

Acknowledgements

This work was supported by the Solar-to-Products program, project number 733.000.003, co-financed by the Netherlands Organization for Scientific Research (NWO) and by ‘Shell Global Solutions International B.V, and by the European Commission (Innovative Training Network ELCOREL, 722614-ELCOREL).

References

- X. Cheng, Z. Shi, N. Glass, L. Zhang, J. Zhang, D. Song, Z.-S. Liu, H. Wang and J. Shen, A review of PEM hydrogen fuel cell contamination: Impacts, mechanisms, and mitigation, *J. Power Sources*, 2007, **165**, 739–756, IBA - HBC 2006.
- J. Feliu, J. Orts, R. Gómez, A. Aldaz and J. Clavilier, New information on the unusual adsorption states of Pt(111) in sulphuric acid solutions from potentiostatic adsorbate replacement by CO, *J. Electroanal. Chem.*, 1994, **372**, 265–268.
- V. Climent, R. Gómez and J. M. Feliu, Effect of increasing amount of steps on the potential of zero total charge of Pt(111) electrodes, *Electrochim. Acta*, 1999, **45**, 629–637.
- T. Nagel, N. Bogolowski and H. Baltruschat, Towards a determination of the active surface area of polycrystalline and nanoparticle electrodes by Cu upd and CO oxidation, *J. Appl. Electrochem.*, 2006, **36**, 1297–1306.
- F. Zhang and A. C. Co, Direct Evidence of Local pH Change and the Role of Alkali Cation during CO₂ Electroreduction in Aqueous Media, *Angew. Chem., Int. Ed.*, 2020, **59**, 1674–1681.
- A. Goyal, G. Marcandalli, V. A. Mints and M. T. M. Koper, Competition between CO₂ Reduction and Hydrogen Evolution on a Gold Electrode under Well-Defined Mass Transport Conditions, *J. Am. Chem. Soc.*, 2020, **142**, 4154–4161.
- B. Hammer, Y. Morikawa and J. K. Nørskov, CO Chemisorption at Metal Surfaces and Overlayers, *Phys. Rev. Lett.*, 1996, **76**, 2141–2144.

- 8 H. Kita, K. Shimazu and K. Kunimatsu, Electrochemical oxidation of CO on Pt in acidic and alkaline solutions: Part I. voltammetric study on the adsorbed species and effects of aging and Sn(IV) pretreatment, *J. Electroanal. Chem. Interfacial Electrochem.*, 1988, **241**, 163–179.
- 9 B. N. Grgur, N. M. Marković, C. A. Lucas and P. J. N. Ross, Electrochemical oxidation of carbon monoxide: From platinum single crystals to low temperature fuel cells catalysts. Part I: Carbon monoxide oxidation onto low index platinum single crystals, *J. Serb. Chem. Soc.*, 2001, **66**, 785–797.
- 10 B. Álvarez, V. Climent, A. Rodes and J. Feliu, Anion adsorption on Pd–Pt(111) electrodes in sulphuric acid solution, *J. Electroanal. Chem.*, 2001, **497**, 125–138.
- 11 H. Kita, H. Nakajima and K. Hayashi, Electrochemical oxidation of CO on Au in alkaline solution, *J. Electroanal. Chem. Interfacial Electrochem.*, 1985, **190**, 141–156.
- 12 P. Rodríguez, A. Koverga and M. Koper, Carbon Monoxide as a Promoter for its own Oxidation on a Gold Electrode, *Angew. Chem., Int. Ed.*, 2010, **49**, 1241–1243.
- 13 G. J. Edens, A. Hamelin and M. J. Weaver, Mechanism of Carbon Monoxide Electrooxidation on Monocrystalline Gold Surfaces: Identification of a Hydroxycarbonyl Intermediate, *J. Phys. Chem.*, 1996, **100**, 2322–2329.
- 14 S. C. Chang, A. Hamelin and M. J. Weaver, Dependence of the electrooxidation rates of carbon monoxide at gold on the surface crystallographic orientation: a combined kinetic-surface infrared spectroscopic study, *J. Phys. Chem.*, 1991, **95**, 5560–5567.
- 15 G. Marcandalli, M. Villalba and M. T. M. Koper, The Importance of Acid-Base Equilibria in Bicarbonate Electrolytes for CO₂ Electrochemical Reduction and CO Reoxidation Studied on Au(hkl) Electrodes, *Langmuir*, 2021, **37**, 5707–5716.
- 16 M. C. O. Monteiro, L. Jacobse and M. T. M. Koper, Understanding the Voltammetry of Bulk CO Electrooxidation in Neutral Media through Combined SECM Measurements, *J. Phys. Chem. Lett.*, 2020, **11**, 9708–9713.
- 17 M. Lukaszewski, M. Soszko and A. Czerwiński, Electrochemical Methods of Real Surface Area Determination of Noble Metal Electrodes – an Overview, *Int. J. Electrochem. Sci.*, 2016, **11**, 4442–4469.
- 18 Q.-S. Chen, J. Solla-Gullón, S.-G. Sun and J. M. Feliu, The potential of zero total charge of Pt nanoparticles and polycrystalline electrodes with different surface structure: The role of anion adsorption in fundamental electrocatalysis, *Electrochim. Acta*, 2010, **55**, 7982–7994.
- 19 A. J. Bard and L. R. Faulkner, *Electrochemical Methods: Fundamentals and Applications*, John Wiley & Sons, 2nd edn, 2000.
- 20 S. Yang and D. G. H. Hetterscheid, Redefinition of the Active Species and the Mechanism of the Oxygen Evolution Reaction on Gold Oxide, *ACS Catal.*, 2020, **10**, 12582–12589.
- 21 R. G. Compton and R. G. Harland, Rotating-disc electrodes and the theory of CE processes. Arbitrary rate constants and diffusion coefficients, *J. Chem. Soc., Faraday Trans. 1*, 1989, **85**, 761–771.
- 22 S. Rebouillat, M. E. G. Lyons and T. Bannon, Evaluation of the proton transfer kinetics of potential electrolytes in non-aqueous solutions using electrochemical techniques Part 1. Kinetic analysis of the general CE mechanism at stationary and rotating electrodes, *J. Solid State Electrochem.*, 1999, **3**, 215–230.
- 23 K.-i. Ataka, T. Yotsuyanagi and M. Osawa, Potential-Dependent Reorientation of Water Molecules at an Electrode/Electrolyte Interface Studied by Surface-Enhanced Infrared Absorption Spectroscopy. The, *J. Phys. Chem.*, 1996, **100**, 10664–10672.
- 24 M. Dunwell, Y. Yan and B. Xu, A surface-enhanced infrared absorption spectroscopic study of pH dependent water adsorption on Au, *Surf. Sci.*, 2016, **650**, 51–56, The surface science of heterogeneous catalysis: In honor of Robert J. Madix.
- 25 K. Arihara, F. Kitamura, T. Ohsaka and K. Tokuda, Characterization of the adsorption state of carbonate ions at the Au(111) electrode surface using in situ IRAS, *J. Electroanal. Chem.*, 2001, **510**, 128–135.
- 26 M. Yaguchi, T. Uchida, K. Motobayashi and M. Osawa, Speciation of Adsorbed Phosphate at Gold Electrodes: A Combined Surface-Enhanced Infrared Absorption Spectroscopy and DFT Study, *J. Phys. Chem. Lett.*, 2016, **7**, 3097–3102.
- 27 R. Martínez-Hincapié, A. Berná, A. Rodes, V. Climent and J. M. Feliu, Surface Acid-Base Properties of Anion-Adsorbed Species at Pt(111) Electrode Surfaces in Contact with CO₂-Containing Perchloric Acid Solutions. The, *J. Phys. Chem. C*, 2016, **120**, 16191–16199.
- 28 M. Auinger, I. Katsounaros, J. C. Meier, S. O. Klemm, P. U. Biedermann, A. A. Topalov, M. Rohwerder and K. J. J. Mayrhofer, Near-surface ion distribution and buffer effects during electrochemical reactions, *Phys. Chem. Chem. Phys.*, 2011, **13**, 16384–16394.
- 29 W. Huang, H. Wang, J. Zhou, J. Wang, P. N. Duchesne, D. Muir, P. Zhang, N. Han, F. Zhao, M. Zeng, J. Zhong, C. Jin, Y. Li, S.-T. Lee and H. Dai, Highly active and durable methanol oxidation electrocatalyst based on the synergy of platinum-nickel hydroxide-graphene, *Nat. Commun.*, 2015, **6**, 10035.
- 30 A. Bach Delpeuch, M. Chatenet, M. S. Rau and C. Cremers, Influence of H- and OH-adsorbates on the ethanol oxidation reaction – a DEMS study, *Phys. Chem. Chem. Phys.*, 2015, **17**, 10881–10893.
- 31 H.-I. Liu, F. Nosheen and X. Wang, Noble metal alloy complex nanostructures: controllable synthesis and their electrochemical property, *Chem. Soc. Rev.*, 2015, **44**, 3056–3078.